THE JOURNAL OF PHYSICAL CHEMISTRY Letters

Letter

Cite This: J. Phys. Chem. Lett. 2019, 10, 3453−3458

pubs.acs.org/JPCL

# Modularized Tuning of Charge Transport through Highly Twisted and Localized Single-Molecule Junctions

Zhixin Chen,[†] Lijue Chen,[†] Jiangpeng Liu, Ruihao Li, Chun Tang, Yuhui Hua, Lichuan Chen, Jia Shi, Yang Yang, Junyang Liu, Jueting Zheng, Lina Chen, Jiankang Cao, Hang Chen, Haiping Xia,* and Wenjing Hong*

State Key Laboratory of Physical Chemistry of Solid Surfaces, College of Chemistry and Chemical Engineering, Collaborative Innovation Center of Chemistry for Energy Materials (iChEM), Xiamen University, Xiamen 361005, China

Supporting Information

**ABSTRACT:** Although most molecular electronic devices and materials consist of a backbone with a planar structure, twisted molecular wires with reduced inter-ring $\pi$-orbital overlap offer a unique opportunity for the modularized fabrication of molecular electronic devices. Herein we investigate the modularized tuning of the charge transport through the localized molecules by designing highly twisted molecules and investigating their single-molecule charge transport using the scanning tunneling microscopy break junction technique. We find that the anthracenediyl-core molecule with a 90° inter-ring twist angle shows an unexpectedly high conductance value, which is five times higher than that of the phenylene-core molecule with a similar configuration, whereas the conductance of the delocalized planar molecule with an anthracenediyl core or a phenylene core is almost the same. Theoretical calculations revealed that highly twisted angles result in weak interactions between molecular building blocks, for which molecule orbitals are separated into localized blocks, which offers the chance for the modularized tuning of every single block. Our findings offer a new strategy for the design of future molecular devices with a localized electronic structure.

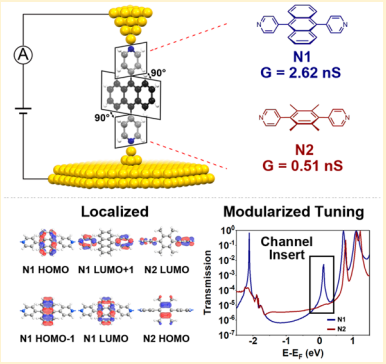


The electronic coupling between different molecular building blocks is essential for the design and fabrication of molecular materials and devices.[1−3] In the current stage, most molecular electronic devices select molecules with a planar structure as building blocks,[4−8] which is mainly because the charge transport through the twisted molecular wires significantly decreases with the increasing twist angle owing to the reduction of inter-ring $\pi$-orbital overlap.[9−12] However, the delocalized electronic structure and strong coupling between building blocks also bring huge challenges for the rational and modularized tuning of charge transport in individual building blocks. To minimize the delocalization for the modularized fabrication of molecular devices, a large twist angle is typically employed to reduce the inter-ring coupling.[13−16] Although the highly twisted molecular wires exhibit a weaker charge-transport ability owing to the weak $\pi$-orbital overlap,[17−21] the weak coupling between each block of molecules with a large inter-ring twist angle results in a highly localized electronic structure. Compared with conjugated molecules with a delocalized electronic structure, molecules with a localized electronic structure exhibit unique quantum phenomena, such as rectification, Coulomb blockade, and negative differential resistance;[22−25] more importantly, the localization of the electronic structure makes it possible to modify a single building block of molecules without perturbation from other building blocks.[13−15] Thus highly twisted molecules with a localized electronic structure may offer a unique chance for the modularized tuning of charge transport by modifying individual building blocks of molecular devices.

In this work, we synthesized and investigated the charge-transport properties through a set of highly twisted molecules with an anthracenediyl core and with a phenylene core using the scanning tunneling microscope break junction (STM-BJ) technique (Figure 1a).[26] **N1** and **N2** were designed with a twist angle of 90° between anchoring groups and central groups to minimize the $\pi$-conjugation between molecular building blocks, and the highly twisted angle leads to the electronic localization of the central group. The single-molecule conductance measurements reveal that the highly twisted and localized **N1** and **N2** exhibit more remarkable conductance tuning than that of **N1A** and **N2A** (Figure 1f) with a planar conjugated structure. Combined density functional theory (DFT) calculations revealed that the localized electronic structure of **N1** allows the insertion of new resonance in the transmission at Fermi energy, whereas the insertion of a new resonance orbital leads to the reorganization of the electronic structure in **N1A** and **N2A** due to the delocalization.

**Received:** March 20, 2019
**Accepted:** June 5, 2019
**Published:** June 5, 2019






DOI: 10.1021/acs.jpclett.9b00796
J. Phys. Chem. Lett. 2019, 10, 3453−3458

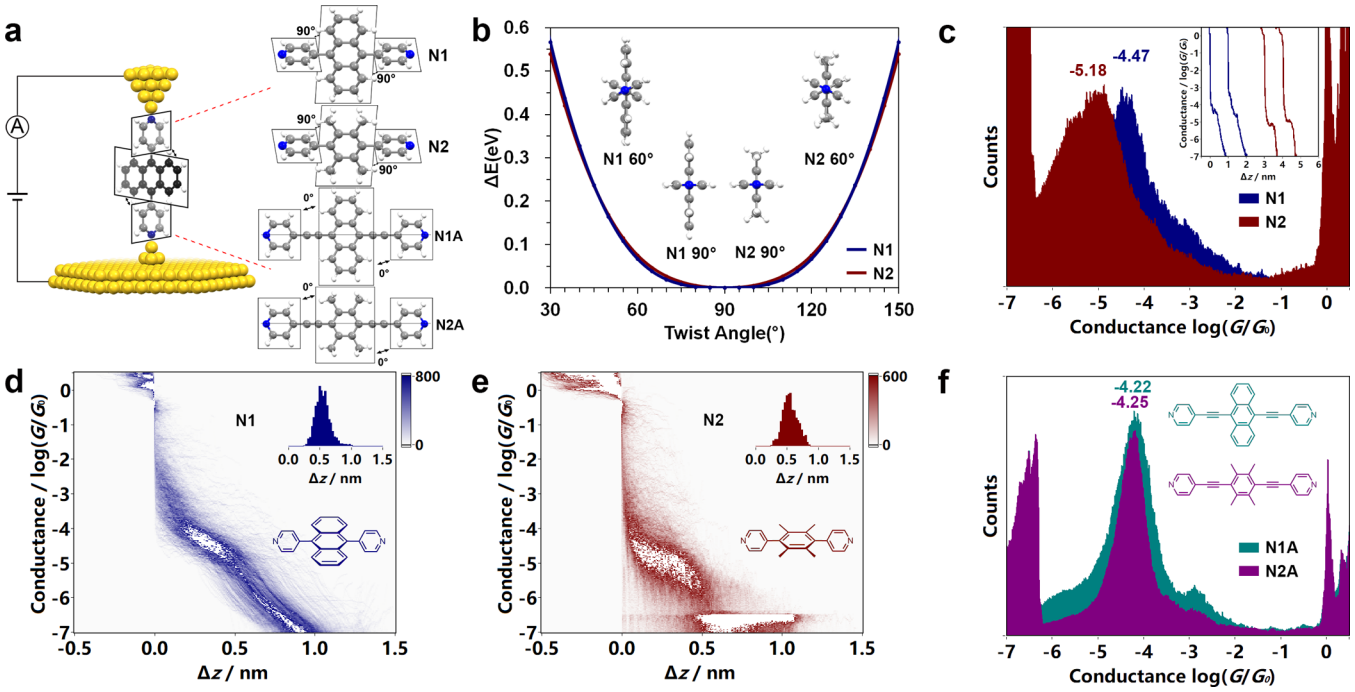


**Figure 1.** (a) Schematic of STM-BJ setup and molecular configurations of **N1**, **N2**, **N1A**, and **N2A**. (b) Comparison of rotational barriers between **N1** (blue) and **N2** (red) and calculated molecular configurations (insert) at twist angles of 90 and 60° (view along the rotational axis). (c) 1D conductance histogram comparisons and typical individual conductance−distance traces (insert) of **N1** (blue) and **N2** (red). 2D conductance versus relative distance ($\Delta z$) histogram and relative distance distributions (insert) of (d) **N1** and (e) **N2**. The relative distance distributions are determined from the conductance ranges of $10^{-0.3}G_0 \approx 10^{-5.1}G_0$ for **N1** and $10^{-0.3}G_0 \approx 10^{-6.2}G_0$ for **N2**. (f) 1D conductance histogram comparisons and chemical structures (insert) of **N1A** (cyan) and **N2A** (magenta).

The target compounds **N1** and **N2** (Figure 1a) were synthesized via Suzuki cross-coupling reactions[27,28] and purified via column chromatography and recrystallization. **N1** and **N2** are composed of three parts, anchoring group−central group−anchoring group (A−C−A), in which the anchoring groups of 4-pyridyl are directly attached to the central aromatic ring without linkers. The central group is 9,10-anthracenediyl in **N1** and 2,3,5,6-tetramethyl-1,4-phenylene in **N2**. Because of the large stereohindrance of the anthracene ring in **N1** or the four methyls in **N2**, the twist angles between the anchoring group and the central group of the most stable configurations of **N1** and **N2** are 90° according to DFT calculations (Figure 1b). As we can see in Figure 1b, **N1** and **N2** both have the lowest energies at a twist angle of 90°. It is found that the rotational barriers of **N1** and **N2** vary slightly.

Single-molecule conductance measurements were carried out using the STM-BJ technique in solutions of 1 mM concentration of target molecules with a mixed solvent of tetrahydrofuran/1,3,5-trimethylbenzene (THF/TMB $v/v$ = 1:4) at room temperature. A fixed bias voltage of 100 mV was applied between the tip and substrate. Figure 1c show the 1D conductance histograms of **N1** and **N2**, each of which is constructed from more than 1000 individual conductance−distance traces without data selection, respectively. All of these molecules exhibited clear molecular plateaus after the breaking of gold−gold atomic contacts at $G_0$ ($G_0 = 2e^2/h = 77.5\ \mu S$), indicating the formation of single-molecule junctions.[29] The conductance−distance traces in the insert of Figure 1c show typical individual conductance traces of **N1** and **N2**. Statistical analysis demonstrates that the conductance value of **N1** locates at $10^{-4.47}G_0$ (2.62 nS), which is five times higher than that of **N2** at $10^{-5.18}G_0$ (0.512 nS). The conductance of **N2** is consistent with previous studies.[17−21]

The 2D conductance versus relative distance histograms of **N1** and **N2** are shown in Figure 1d,e. It is found that all molecules showed highly distinct conductance intensity clouds, indicating that single-molecule junctions formed during most of the stretching cycles with similar charge-transport properties. Further analysis of the displacement distribution of all of the molecular junctions (insert of Figure 1d,e) suggests that the lengths of these molecular junctions are all determined to be ∼1 nm. (The peak of the length distributions located at ∼0.5 nm and a +0.5 nm calibrated gold−gold snap-back distance should be added.[30]) The lengths of the characterized junctions are in good agreement with the molecular lengths, suggesting that the molecules bridge between the two gold electrodes with a fully stretched configuration. Thus the conductance variation between different molecules originates from the changes of the central ring single-molecule junctions.

To compare the difference of highly twisted molecules with regular planar conjugated molecules, we synthesized **N1A** and **N2A**, shown in Figure 1f, via Sonogashira cross-coupling reactions[31,32] with the same central units of **N1** and **N2**, but ethynylene linkers are inserted between the anchoring groups and central groups, which makes the twist angles between the core and the terminal pyridine plane of the two molecules almost 0°, as depicted in Figure S2. It should be noticed that the ethynylene groups are well conjugated with both pyridyl groups and central groups, which leads to strong coupling between pyridyl groups and central groups. Thus we described the ethynylene groups as "linkers" but not "spacers". As a result of good $\pi$-conjugation, all nonhydrogen atoms were coplanar without the effect of stereohindrance. We find that the



DOI: 10.1021/acs.jpclett.9b00796
J. Phys. Chem. Lett. 2019, 10, 3453−3458

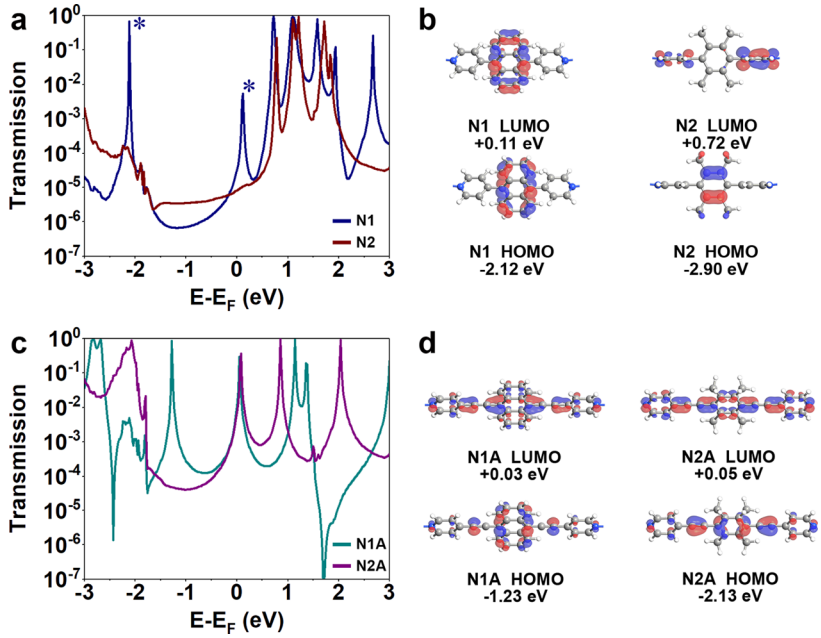


**Figure 2.** Calculated transmission functions of (a) **N1** (blue) and **N2** (red) and (c) **N1A** (cyan) and **N2A** (magenta). Inserted channels in **N1** are labeled by asterisks in panel a. MPSH plots of (b) **N1** and **N2** and (d) **N1A** and **N2A**. The isovalue was set at 0.05 au. Energies are related to the Fermi energy.

conductance of **N1A** and **N2A** varies slightly from $10^{-4.22}G_0$ (4.66 nS) for **N1A** to $10^{-4.25}G_0$ (4.36 nS) for **N2A**, which is consistent with the previous results.[33]

To further reveal why the difference between **N1** and **N2** is significantly larger than that between **N1A** and **N2A**, DFT calculations were performed to calculate the transmission functions through single-molecule junctions. The molecules were first optimized in a vacuum using Gaussian software;[34] then, they were wired into single-molecule junction configurations. The single-molecule junctions were relaxed to a force threshold of 0.05 eV/Å using the DFT code SIESTA[35] with the Perdew−Burke−Ernzerhof (PBE) correlation-exchange functional.[36] The optimized single-molecule junctions were utilized to calculate transmission functions in the ATK software package with nonequilibrium Green's functions (NEGFs).[37−39] More details of the calculations are shown in the Supporting Information. The peaks at the relative energy levels of −2.12 and +0.12 eV are attributed to the HOMO and LUMO of **N1** (labeled by asterisks in Figure 2a). Previous studies revealed that the LUMO is the dominant conductance channel for molecules with an anchoring group of pyridyl.[30] Thus the inserted LUMO of **N1** at +0.11 eV becomes the dominant transport channel, which has a very strong electronic coupling with electrodes (see scattering states plot in Figure S10).[40] The strong coupling between the LUMO of **N1** and the Fermi energy significantly enhanced the charge transport through the single-molecule junctions. In contrast, the LUMO of **N2** is far away from the Fermi energy and shows a lower conductance than **N1** at the Fermi energy.

Molecular projected self-consistent Hamiltonian (MPSH)[41] plots of the frontier molecular orbital were all calculated using the junction configuration, shown in Figure 2b,d (more details in Figure S9), which demonstrates that the major difference in electronic structures between **N1** and **N1A** (or **N2** and **N2A**) is that **N1** and **N2** have localized electronic structures, whereas **N1A** and **N2A** have delocalized electronic structures. As shown in Figure 2b, the LUMO of **N2** is located at the pyridyl groups, whereas the HOMO of **N2** is located at the central group. In contrast with **N2**, the HOMO and LUMO of **N1** are both located at the central group. This separation of frontier molecular orbitals is attributed to the weak inter-ring electronic coupling from the highly twisted configurations, which bridges the widely employed strategy for designing efficient organic light-emitting diodes in which the highly twisted configuration leads to the separation and localization of the HOMO and LUMO.[13−15] In the charge transport through single-molecule junctions, the localized electronic structures of highly twisted molecules offer the chance for the modularized individual tuning of the energy levels of the HOMO and the LUMO.

To reveal why the conductance difference of planar **N1A** and **N2A** becomes much smaller, we further calculated the transmission functions, as shown in Figure 2c. It is found that the energy level of the dominated transport channel of **N1A** is quite similar to that of **N2A**, and the variety from **N2A** to **N1A** is simply the narrowing of the HOMO−LUMO gap, which does not make a remarkable change at the transport channel near the Fermi energy. Frontier molecular orbitals of **N1A** and **N2A** presented in Figure 2b show good continuity, indicating strong electronic coupling between anchoring groups and the central group, which we have mentioned above. As a result, the replacement of the central phenyl group with anthracenediyl would be averaged by electronic delocalization, resulting in the experimental challenge of rational tuning of charge transport in the delocalized single-molecule junction. Further investigations of the charge transport through highly twisted molecules with naphthalenyl, tetracenyl, and pentacenyl were carried out using DFT calculations, as shown in Figures S14−S16. By replacing the central phenyl group with naphthalenyl, anthracenediyl, tetracenyl, or pentacenyl, the transmission at Fermi energy of **N1**, **N2**, **N3**, **N4**, and **N5** gradually increases with the enlarging of conjugation, as shown in Figure S16a. However, the transmission at Fermi energy of **N1A**, **N2A**, **N3A**, **N4A**, and **N5A**, as shown in Figure S16b, remains almost the same, suggesting that the modulation of charge transport in highly



DOI: 10.1021/acs.jpclett.9b00796
J. Phys. Chem. Lett. 2019, 10, 3453−3458

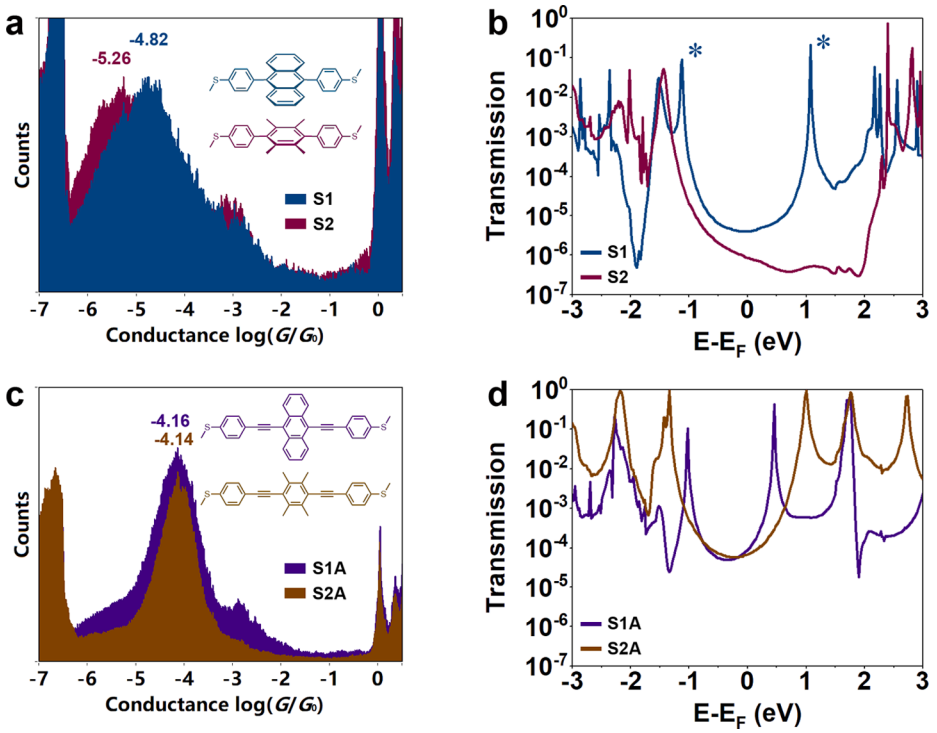


**Figure 3.** 1D conductance histogram comparisons and chemical structures (insert) of (a) **S1** (indigo) and **S2** (amaranth) and (c) **S1A** (purple) and **S2A** (brown). Calculated transmission functions of (b) **S1** (indigo) and **S2** (amaranth) and (d) **S1A** (purple) and **S2A** (brown). Inserted channels in **S1** are labeled by asterisks in panel b.

twisted molecules is more efficient than that of the planar and conjugated molecules while using the same central groups.

To further validate the generalization of the strategy, **S1**, **S2**, **S1A**, and **S2A** were designed by replacing the 4-pyridinyl anchoring groups of **N1**, **N2**, **N1A**, and **N2A** with 4-(methylthio)phenyl. Similarly, weak inter-ring electronic coupling from the highly twisted configuration leads to localized electronic structures of **S1** and **S2**, whereas strong electronic coupling of ethynylene linkers leads to delocalized electronic structures of **S1A** and **S2A** as well. Figure 3a,c shows the conductance histograms of **S1**, **S2** and **S1A**, **S2A**, each of which was constructed from more than 1000 individual conductance−distance traces without data selection, respectively. Statistical analysis demonstrates that the conductance value of **S1** locates at $10^{-4.82}G_0$ (1.17 nS), which is three times higher than that of **S2** at $10^{-5.26}G_0$ (0.426 nS). The conductance of **S1A** and **S2A** varies very slightly from $10^{-4.16}G_0$ (5.36 nS) for **S1A** to $10^{-4.14}G_0$ (5.66 nS) for **S2A**, which is similar to the result of **N1A** and **N2A** and consistent with the previous results.[33] The calculated transmission functions shown in Figure 3b,d indicate that there are two more channels inserted at −1.12 and +1.08 eV with >1 eV of gap from the Fermi energy in the transmission function of **S1**, whereas the variety from **S2A** to **S1A** leads to the narrowing of the HOMO−LUMO gap, as also demonstrated in **N1A** and **N2A**. Thus the charge-transport difference between **S1** and **S2** is obviously larger than that between **S1A** and **S2A**. We also found that the charge transport of **S1** will significantly decrease by replacing the hydrogens with fluorine due to the inductive effect (Figure S12). These results support our hypothesis that the properties of the localization lead to more efficient tuning than that of the delocalized molecules.

In conclusion, we investigated the modularized tuning of charge transport through a family of highly twisted and localized single-molecule junctions using the STM-BJ technique. We found that the highly twisted molecules provided more efficient tuning than planar conjugated molecules and that the conductance of the highly twisted anthracenediyl-core molecule with the 4-pyridinyl anchor is five times higher than that of the highly twisted phenyl-core molecule with 4-pyridinyl anchor, whereas the conductance of the planar anthracenediyl-core molecule is almost the same as that of the planar phenyl-core molecule. A similar trend is observed in the molecules with 4-pyridinyl anchoring groups replaced by 4-(methylthio)phenyl. DFT calculations reveal that the localized electronic structures of highly twisted molecules allow the insertion of resonance in the transmission at Fermi energy via the replacement of the phenylene core in **N2** by the anthracenediyl core in **N1**. Our findings suggest that modifying electronic structures in the highly twisted molecule with a localized electronic structure offers the chance to modulate charge transport at the single-block level, leading to the modularized design of molecular devices and materials.

## ■ ASSOCIATED CONTENT

### Supporting Information

The Supporting Information is available free of charge on the ACS Publications website at DOI: 10.1021/acs.jpclett.9b00796.

1. Synthesis of compounds; 2. NMR spectra of compounds; 3. blank experiment results for pure solvent; 4. additional experimental data; and 5. computational details (PDF)



DOI: 10.1021/acs.jpclett.9b00796
J. Phys. Chem. Lett. 2019, 10, 3453−3458

## AUTHOR INFORMATION


### Corresponding Authors

*E-mail: hpxia@xmu.edu.cn (H.X.).
*E-mail: whong@xmu.edu.cn (W.H.).

### ORCID

Yang Yang: 0000-0003-1967-3398
Junyang Liu: 0000-0002-7252-1900
Haiping Xia: 0000-0002-2688-6634
Wenjing Hong: 0000-0003-4080-6175

### Author Contributions

†Zhixin Chen and Lijue Chen contributed equally to this work.


### Notes

The authors declare no competing financial interest.

## ACKNOWLEDGMENTS

We thank Zhiyong Chen, Hang Qu, Zi-Ang Nan, and Dr. Hongliang Chen for helpful discussion. This work was supported by the National Key R&D Program of China (2017YFA0204902), the National Natural Science Foundation of China (nos. 21673195, 21722305, 21703188, 31871877, U1705254), China Postdoctoral Science Foundation (no. 2017M622060), and the Young Thousand Talent Project of China.

## REFERENCES


(1) Meng, F.; Hervault, Y. M.; Shao, Q.; Hu, B.; Norel, L.; Rigaut, S.; Chen, X. Orthogonally Modulated Molecular Transport Junctions for Resettable Electronic Logic Gates. *Nat. Commun.* **2014**, *5*, 3023.

(2) Su, T. A.; Neupane, M.; Steigerwald, M. L.; Venkataraman, L.; Nuckolls, C. Chemical Principles of Single-Molecule Electronics. *Nat. Rev. Mater.* **2016**, *1*, 16002.

(3) Jia, C.; Guo, X. Molecule-Electrode Interfaces in Molecular Electronic Devices. *Chem. Soc. Rev.* **2013**, *42*, 5642−5660.

(4) Diez-Perez, I.; Li, Z.; Hihath, J.; Li, J.; Zhang, C.; Yang, X.; Zang, L.; Dai, Y.; Feng, X.; Muellen, K.; et al. Gate-Controlled Electron Transport in Coronenes as a Bottom-up Approach Towards Graphene Transistors. *Nat. Commun.* **2010**, *1*, 31.

(5) Garner, M. H.; et al. Comprehensive Suppression of Single-Molecule Conductance Using Destructive Sigma-Interference. *Nature* **2018**, *558*, 415−419.

(6) Li, R.; et al. Switching of Charge Transport Pathways Via Delocalization Changes in Single-Molecule Metallacycles Junctions. *J. Am. Chem. Soc.* **2017**, *139*, 14344−14347.

(7) Tao, N. J. Electron Transport in Molecular Junctions. *Nat. Nanotechnol.* **2006**, *1*, 173−181.

(8) Yang, G.; et al. Protonation Tuning of Quantum Interference in Azulene-Type Single-Molecule Junctions. *Chem. Sci.* **2017**, *8*, 7505−7509.

(9) Dou, K. P.; De Sarkar, A.; Wang, C. L.; Zhang, R. Q. Intramolecular Torsion Based Molecular Switch Functionality Enhanced in Π-Conjugated Oligomolecules by a Π-Conjugated Pendant Group. *J. Phys. Chem. C* **2011**, *115*, 13911−13918.

(10) Finch, C. M.; Sirichantaropass, S.; Bailey, S. W.; Grace, I. M.; García-Suarez, V. M.; Lambert, C. J. Conformation Dependence of Molecular Conductance: Chemistry Versus Geometry. *J. Phys.: Condens. Matter* **2008**, *20*, 022203.

(11) George, C. B.; Ratner, M. A.; Lambert, J. B. Strong Conductance Variation in Conformationally Constrained Oligosilane Tunnel Junctions. *J. Phys. Chem. A* **2009**, *113*, 3876−3880.

(12) Xin, N.; et al. Stereoelectronic Effect-Induced Conductance Switching in Aromatic Chain Single-Molecule Junctions. *Nano Lett.* **2017**, *17*, 856−861.

(13) Kim, D. H.; et al. High-Efficiency Electroluminescence and Amplified Spontaneous Emission from a Thermally Activated Delayed Fluorescent near-Infrared Emitter. *Nat. Photonics* **2018**, *12*, 98−104.

(14) Zhang, Q. S.; Li, B.; Huang, S. P.; Nomura, H.; Tanaka, H.; Adachi, C. Efficient Blue Organic Light-Emitting Diodes Employing Thermally Activated Delayed Fluorescence. *Nat. Photonics* **2014**, *8*, 326−332.

(15) Uoyama, H.; Goushi, K.; Shizu, K.; Nomura, H.; Adachi, C. Highly Efficient Organic Light-Emitting Diodes from Delayed Fluorescence. *Nature* **2012**, *492*, 234−238.

(16) Sisto, T. J.; Zhong, Y.; Zhang, B.; Trinh, M. T.; Miyata, K.; Zhong, X.; Zhu, X. Y.; Steigerwald, M. L.; Ng, F.; Nuckolls, C. Long, Atomically Precise Donor-Acceptor Cove-Edge Nanoribbons as Electron Acceptors. *J. Am. Chem. Soc.* **2017**, *139*, 5648−5651.

(17) Venkataraman, L.; Klare, J. E.; Nuckolls, C.; Hybertsen, M. S.; Steigerwald, M. L. Dependence of Single-Molecule Junction Conductance on Molecular Conformation. *Nature* **2006**, *442*, 904−907.

(18) Vonlanthen, D.; Mishchenko, A.; Elbing, M.; Neuburger, M.; Wandlowski, T.; Mayor, M. Chemically Controlled Conductivity: Torsion-Angle Dependence in a Single-Molecule Biphenyldithiol Junction. *Angew. Chem., Int. Ed.* **2009**, *48*, 8886−8890.

(19) Mishchenko, A.; et al. Influence of Conformation on Conductance of Biphenyl-Dithiol Single-Molecule Contacts. *Nano Lett.* **2010**, *10*, 156−163.

(20) Cui, L.; Liu, B.; Vonlanthen, D.; Mayor, M.; Fu, Y.; Li, J.-F.; Wandlowski, T. In Situ Gap-Mode Raman Spectroscopy on Single-Crystal Au(100) Electrodes: Tuning the Torsion Angle of 4,4′-Biphenyldithiols by an Electrochemical Gate Field. *J. Am. Chem. Soc.* **2011**, *133*, 7332−7335.

(21) Bi, H.; Palma, C.-A.; Gong, Y.; Hasch, P.; Elbing, M.; Mayor, M.; Reichert, J.; Barth, J. V. Voltage-Driven Conformational Switching with Distinct Raman Signature in a Single-Molecule Junction. *J. Am. Chem. Soc.* **2018**, *140*, 4835−4840.

(22) Yuan, L.; Wang, L. J.; Garrigues, A. R.; Jiang, L.; Annadata, H. V.; Anguera Antonana, M.; Barco, E.; Nijhuis, C. A. Transition from Direct to Inverted Charge Transport Marcus Regions in Molecular Junctions Via Molecular Orbital Gating. *Nat. Nanotechnol.* **2018**, *13*, 322−329.

(23) Lovat, G.; Choi, B.; Paley, D. W.; Steigerwald, M. L.; Venkataraman, L.; Roy, X. Room-Temperature Current Blockade in Atomically Defined Single-Cluster Junctions. *Nat. Nanotechnol.* **2017**, *12*, 1050−1054.

(24) Kubatkin, S.; Danilov, A.; Hjort, M.; Cornil, J.; Bredas, J. L.; Stuhr-Hansen, N.; Hedegard, P.; Bjornholm, T. Single-Electron Transistor of a Single Organic Molecule with Access to Several Redox States. *Nature* **2003**, *425*, 698−701.

(25) Perrin, M. L.; Galan, E.; Eelkema, R.; Thijssen, J. M.; Grozema, F.; van der Zant, H. S. J. A Gate-Tunable Single-Molecule Diode. *Nanoscale* **2016**, *8*, 8919−8923.

(26) Xu, B.; Tao, N. J. Measurement of Single-Molecule Resistance by Repeated Formation of Molecular Junctions. *Science* **2003**, *301*, 1221−1223.

(27) Fudickar, W.; Linker, T. Synthesis of Pyridylanthracenes and Their Reversible Reaction with Singlet Oxygen to Endoperoxides. *J. Org. Chem.* **2017**, *82*, 9258−9262.

(28) Scott, H. S.; Shivanna, M.; Bajpai, A.; Chen, K.-J.; Madden, D. G.; Perry, J. J., IV; Zaworotko, M. J. Enhanced Stability toward Humidity in a Family of Hybrid Ultramicroporous Materials Incorporating $Cr_2O_7^{2-}$ Pillars. *Cryst. Growth Des.* **2017**, *17*, 1933−1937.

(29) Huang, C.; Rudnev, A. V.; Hong, W.; Wandlowski, T. Break Junction under Electrochemical Gating: Testbed for Single-Molecule Electronics. *Chem. Soc. Rev.* **2015**, *44*, 889−901.

(30) Hong, W.; Manrique, D. Z.; Moreno-García, P.; Gulcur, M.; Mishchenko, A.; Lambert, C. J.; Bryce, M. R.; Wandlowski, T. Single Molecular Conductance of Tolanes: Experimental and Theoretical Study on the Junction Evolution Dependent on the Anchoring Group. *J. Am. Chem. Soc.* **2012**, *134*, 2292−2304.

(31) Karagiaridi, O.; Bury, W.; Tylianakis, E.; Sarjeant, A. A.; Hupp, J. T.; Farha, O. K. Opening Metal−Organic Frameworks Vol. 2: Inserting Longer Pillars into Pillared-Paddlewheel Structures through




DOI: 10.1021/acs.jpclett.9b00796
J. Phys. Chem. Lett. 2019, 10, 3453−3458

Solvent-Assisted Linker Exchange. *Chem. Mater.* **2013**, *25*, 3499−3503.
(32) Fasina, T. M.; et al. Synthesis, Optical Properties, Crystal Structures and Phase Behaviour of Selectively Fluorinated 1,4-Bis(4′-Pyridylethynyl)Benzenes, 4-(Phenylethynyl)Pyridines and 9,10-Bis-(4′-Pyridylethynyl)Anthracene, and a $Zn(NO_3)_2$ Coordination Polymer. *J. Mater. Chem.* **2004**, *14*, 2395−2404.
(33) Kaliginedi, V.; Moreno-García, P.; Valkenier, H.; Hong, W.; García-Suárez, V. M.; Buiter, P.; Otten, J. L. H.; Hummelen, J. C.; Lambert, C. J.; Wandlowski, T. Correlations between Molecular Structure and Single-Junction Conductance: A Case Study with Oligo(Phenylene-Ethynylene)-Type Wires. *J. Am. Chem. Soc.* **2012**, *134*, 5262−5275.
(34) Frisch, M. J.; et al. *Gaussian 16*, rev. B.01; Gaussian, Inc.: Wallingford, CT, 2016.
(35) Soler, J. M.; Artacho, E.; Gale, J. D.; García, A.; Junquera, J.; Ordejón, P.; Sánchez-Portal, D. The Siesta Method for Ab Initio Order-N Materials Simulation. *J. Phys.: Condens. Matter* **2002**, *14*, 2745−2779.
(36) Perdew, J. P.; Burke, K.; Ernzerhof, M. Generalized Gradient Approximation Made Simple. *Phys. Rev. Lett.* **1996**, *77*, 3865−3868.
(37) Brandbyge, M.; Mozos, J. L.; Ordejon, P.; Taylor, J.; Stokbro, K. Density-Functional Method for Nonequilibrium Electron Transport. *Phys. Rev. B: Condens. Matter Mater. Phys.* **2002**, *65*, 165401.
(38) Fan, Z. Q.; Chen, K. Q. Negative Differential Resistance and Rectifying Behaviors in Phenalenyl Molecular Device with Different Contact Geometries. *Appl. Phys. Lett.* **2010**, *96*, 053509.
(39) Capozzi, B.; Xia, J. L.; Adak, O.; Dell, E. J.; Liu, Z. F.; Taylor, J. C.; Neaton, J. B.; Campos, L. M.; Venkataraman, L. Single-Molecule Diodes with High Rectification Ratios through Environmental Control. *Nat. Nanotechnol.* **2015**, *10*, 522−527.
(40) Zang, Y. P.; Pinkard, A.; Liu, Z. F.; Neaton, J. B.; Steigerwald, M. L.; Roy, X.; Venkataraman, L. Electronically Transparent Au-N Bonds for Molecular Junctions. *J. Am. Chem. Soc.* **2017**, *139*, 14845−14848.
(41) Stokbro, K.; Taylor, J.; Brandbyge, M.; Mozos, J. L.; Ordejon, P. Theoretical Study of the Nonlinear Conductance of Di-Thiol Benzene Coupled to Au(111) Surfaces Via Thiol and Thiolate Bonds. *Comput. Mater. Sci.* **2003**, *27*, 151−160.



DOI: 10.1021/acs.jpclett.9b00796
*J. Phys. Chem. Lett.* 2019, 10, 3453−3458